FACULTY OF MECHANICAL ENGINEERING CTU IN PRAGUE

DEPARTMENT OF ENVIRONMENTAL ENGINEERING

UNIVERSITY CENTRE FOR ENERGY EFFICIENT BUILDINGS CTU IN PRAGUE

TITLE

TRNSYS TYPE 205

MODEL OF GLAZED SOLAR LIQUID COLLECTOR BASED ON DETAILED CONSTRUCTION PARAMETERS AND ENERGY BALANCE

AUTHORS Viacheslav Shemelin

Tomáš Matuška

PAGES 34

ANNEXES 1

DATE November 2017

Contents

1 Introduction

The presented type 205 is a detailed mathematical model developed for a typical flat-plate collector implemented into TRNSYS simulation software. The type is a successor of design tool KOLEKTOR 2.0 [1] originally programmed in Visual Basic as separately executable program.

Considered flat-plate collector consists of an absorber in the insulated box covered with transparent cover. There is an air gap between the absorber and cover and absorber and back insulation, both defined by thickness and slope. The absorber design is either harp consisting from distribution pipes and risers pipes (defined by length, distance and diameter) or fully wetted consisting from distribution channels and risers channels (defined by length, width and height of the channels). Transparent cover (glazing or transparent insulation structure) and back thermal insulation are defined by temperature dependent thermal conductance. Heat transfer liquid can be chosen from water, ethyleneglycol-water mixture and propyleneglycol-water mixture.

The detailed model of flat-plate solar collector allows a detailed calculation of heat transfer in the solar collector. Energy flow from the absorber surface to ambient and from the absorber surface into heat transfer liquid and temperature distribution in the collector are calculated in the iteration loops. Solar collector can be specified by a number of detailed parameters, optical properties of glazing and absorber, thermophysical properties of main components of solar collector (frame, absorber, transparent cover).

The implementation of the model in TRNSYS environment offers the parametric analyses for different construction alternatives for annual solar collector performance in given solar system application. There is also a possibility to change a mathematical models describing the fundamental heat transfer phenomena (closed gap convection, wind convection, forced convection heat transfer on pipes etc.) and make sensitivity analyses for selection of the models.

2 Parameter-List

Nr.	***short***	***explanation***	***unit***	***range***
1	K	Collector length	m	[0;inf]
2	H	Collector width	m	[0;inf]
3	B	Collector height	m	[0;inf]
4	A_{abs}	Absorber area	m^2	[0;inf]
5	d_f	Absorber-cover gap thickness	mm	[0;inf]
6	h_{cov0}	Thermal conductance of cover 0	$W/m^2.K$	[0;inf]
7	h_{cov1}	Thermal conductance of cover 1	$W/m^2.K^2$	[-inf;inf]
8	h_{cov2}	Thermal conductance of cover 2	$W/m^2.K^3$	[-inf;inf]
9	$\varepsilon_{abs,f}$	Front surface emissivity of absorber	[-]	[0;1]
10	$\varepsilon_{abs,b}$	Back surface emissivity of absorber	[-]	[0;1]
11	ε_{c1}	Internal surface emissivity of cover (f_1)	[-]	[0;1]
12	ε_{c2}	External surface emissivity of cover (f_2)	[-]	[0;1]
13	d_b	Absorber-insulation gap thickness	mm	[0;inf]
14	h_{ins0}	Thermal conductance of back insulation 0	$W/m^2.K$	[0;inf]

Parameter list *(Continued)*

15	h_{ins1}	Thermal conductance of back insulation 1	$W/m^2.K^2$	[-inf;inf]
16	h_{ins2}	Thermal conductance of back insulation 2	$W/m^2.K^3$	[-inf;inf]
17	h_{edge0}	Thermal conductance of edge insulation 0	$W/m^2.K$	[0;inf]
18	h_{edge1}	Thermal conductance of edge insulation 1	$W/m^2.K^2$	[-inf;inf]
19	h_{edge2}	Thermal conductance of edge insulation 2	$W/m^2.K^3$	[-inf;inf]
20	ε_{ins}	Internal surface emissivity of insulation (b_1)	[-]	[0;1]
21	ε_{fs}	External surface emissivity of frame (b_2)	[-]	[0;1]
22	ε_{as}	Emissivity of adjacent surfaces	[-]	[0;1]
23	d_{abs}	Thickness of absorber	mm	[0;inf]
24	λ_{abs}	Thermal conductivity of absorber	$W/m.K$	[0;inf]
25	W	Distance between riser pipes	mm	[0;inf]
26	L	Length of riser pipes or fluid channels	m	[0;inf]
27	D_e	Riser pipe external diameter	mm	[0;inf]
28	D_i	Riser pipe internal diameter	mm	[0;inf]
29	a	Average bond width or fluid channels width	mm	[0;inf]
30	b	Average bond thickness or fluid channels height	mm	[0;inf]
31	λ_b	Bond thermal conductivity	$W/m.K$	[0;inf]
32	P	Number of riser pipes or fluid channels	[-]	[0;inf]
33	τ_n	Solar transmittance of the collector cover	[-]	[0;1]
34	α_{abs}	Solar absorptance of the absorber	[-]	[0;1]
35	b_0	1st-order incidence angle modifier (IAM)	[-]	[0;1]
36	b_1	2nd-order incidence angle modifier (IAM)	[-]	[-1;1]
37	M_1	Wind convection model Mode	[-]	[1;4]
38	M_2	Front gap convection model Mode	[-]	[1;6]
39	M_3	Heat transfer fluids model Mode	[-]	[1;3]
40	M_4	Glycol mass concentration	[%]	[0;100]
41	M_5	Absorber configuration Mode	[-]	[1;4]
42	M_6	Laminar convection heat transfer in pipes model	[-]	[1;5]
43	M_7	Turbulent convection heat transfer in pipes model	[-]	[1;6]

3 Input-List

Nr.	***short***	***explanation***	***unit***	***range***
1	t_{in}	Inlet fluid temperature	$°C$	[-inf;+inf]
2	$\dot{M}$	Inlet fluid flowrate	kg/h	[0;inf]
3	t_{amb}	Ambient temperature	$°C$	[-inf;+inf]
4	t_{sky}	Sky temperature	$°C$	[-inf;+inf]
5	I_{beam}	Beam radiation for collector surface	$kJ/h.m^2$	[0;inf]
6	I_{sky}	Sky diffuse radiation for collector surface	$kJ/h.m^2$	[0;inf]
7	I_{gnd}	Ground reflected diffuse radiation for collector surface	$kJ/h.m^2$	[0;inf]
8	θ	Incidence angle	deg	[0;+inf]
9	φ	Collector slope	deg	[0;90]
10	w	Wind velocity	m/s	[0;+inf]

4 Output-List

Nr.	*short*	*explanation*	*unit*	*range*
1	t_{out}	Outlet fluid temperature	*°C*	[-inf;+inf]
2	$\dot{M}$	Outlet fluid flowrate	*kg/h*	[0;inf]
3	Φ_{out}	Useful energy gain of collector	*kJ/h*	[-inf;+inf]
4	η	Collector thermal efficiency	[-]	[0;1]
5	t_{abs}	Absorber temperature	*°C*	[-inf;+inf]
6	t_{mean}	Mean fluid temperature	*°C*	[-inf;+inf]
7	U	Overall heat loss coefficient of collector	$W/m^2.K$	[0;inf]

5 Units conversion

In the table above, there are several non-SI units. The presented type 205 computes in the SI units, which are more convenient for calculations. Therefore all non-SI units have to be converted into SI units. The conversion of some non-SI units into SI units is given in Tab. 1.

Tab. 1 - Conversation of non-SI units

Dimension	Non-SI unit	Equivalence in SI-units
Temperature	t [°C]	$\vartheta = t + 273.15$ [K]
Mass flow	$\dot{M}$ [kg/h]	$\dot{m} = \frac{\dot{M}}{3600}$ [kg/s]
Energy flux	I [kJ/h.m^2]	$G = \frac{I}{3.6}$ [W/m^2]
Power	Φ_{out} [kJ/h]	$\dot{Q}_u = \frac{\Phi_{out}}{3.6}$ [W]

6 Basic Equations

The core of the type 205 is a mathematical model for solar flat-plate liquid collector solving one-dimensional heat transfer balances. Hottel and Woertz [2], Hottel and Whilier [3] and Bliss [4] developed the simplest assumptions: thermal capacitances are neglected and a single value of collector overall heat loss coefficient is considered, which depends on collector characteristics (geometry, mass flow rate, efficiency itself etc.), average plate temperature and external conditions (air, temperature and external heat transfer coefficient). Based on these assumptions and considering that the heat transfer is mainly one-dimensional and predominant in the direction normal to the flow plane, Duffie and Beckman [5] developed a simplified model to characterize the solar collector in steady state conditions.

The mathematical model in general consists of two parts: external energy balance of absorber (heat transfer from absorber surface to ambient environment) and internal energy balance of absorber (heat transfer from absorber surface into heat transfer fluid). Model solves the energy balance of the solar collector under steady-state conditions according to principle Hottel-Whillier equation for usable thermal power

$$\dot{Q}_u = A_{abs} F_R \left[\tau_n \alpha_{abs} G_t - U\left(\vartheta_{in} - \vartheta_{amb}\right)\right] \quad [\mathrm{W}] \qquad (1)$$

A literature review to find appropriate theoretical and empirical relationships for heat transfer coefficients calculation has been done by Matuska [6]. For certain heat transfer phenomena, a number of equations exist from different sources. Detailed description of the heat transfer models can be found in [1].

The main planes of the collector are cover exterior surface (f_2), cover interior surface (f_1), absorber (*abs*), back insulation interior surface (b_1), back frame exterior surface (b_2), edge insulation interior surface (e_1) and edge frame exterior surface (e_2). Ambient environment is labeled with (*amb*). A surface temperature is determined for each plane of collector during the calculation procedure. The main collector planes are schematically outlined in Fig. 1.

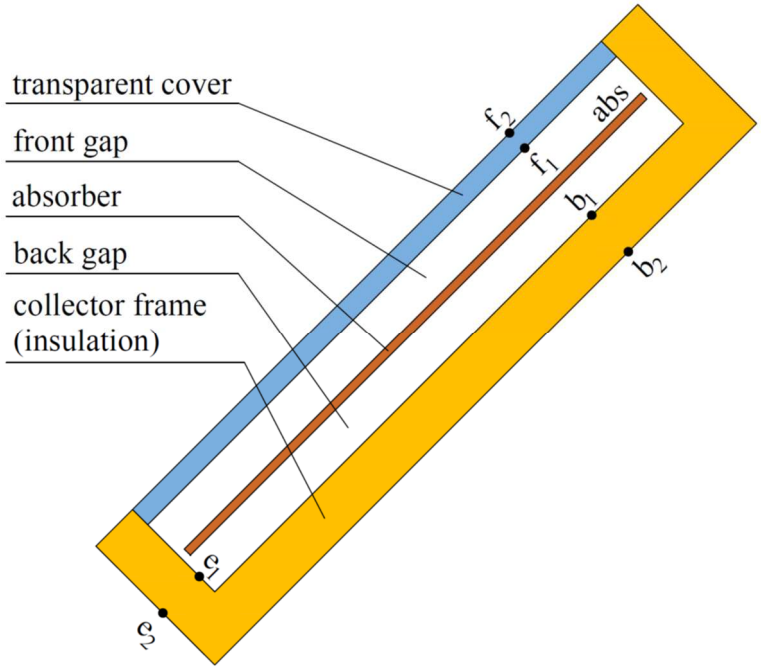

Fig. 1 – Main temperature planes (surfaces) in solar collector model

6.1 External energy balance

The external energy balance consists of:

1) the heat transfer by radiation and by natural convection in the gap between absorber surface and transparent cover (respectively back insulation and edge insulation);
2) the heat transfer by conduction through transparent cover (respectively back insulation and edge insulation);
3) the heat transfer convection and radiation from exterior cover (respectively back frame and edge frame) surface to ambient.

To calculate the heat transfer coefficients properly, temperatures for main collector planes (surfaces) should be known, but on the other side the temperature distribution in the collector is dependent on the heat transfer coefficients values. Therefore, external energy balance of absorber is solved in an iteration loop starting from first estimate of temperatures for each main surface based on given input temperature ϑ_{in} and ambient temperature ϑ_{amb}. The absorber

temperature ϑ_{abs} required in the calculation is estimated in first iteration loop of external balance from ϑ_{in} by relationship:

$$\vartheta_{abs} = \vartheta_{in} + 10 \qquad [\mathrm{K}] \tag{2}$$

Then for the calculation of heat transfer coefficients between main collector surfaces (f_1, f_2, b_1, b_2, e_1, e_2), the surface temperatures are needed, but at the start of calculation process the temperatures are not known. In the first iteration step, surface temperatures are estimated from temperature difference between absorber and ambient environment uniformly as follows:

$$\vartheta_{f1} = \vartheta_{b1} = \vartheta_{e1} = \vartheta_{abs} - \frac{\vartheta_{abs} - \vartheta_{amb}}{3} \qquad [\mathrm{K}] \tag{3}$$

$$\vartheta_{f2} = \vartheta_{b2} = \vartheta_{e2} = \vartheta_{amb} + \frac{\vartheta_{abs} - \vartheta_{amb}}{3} \qquad [\mathrm{K}] \tag{4}$$

After that heat transfer coefficients can be calculated and collector heat loss coefficients U_f, U_b and U_e can be obtained.

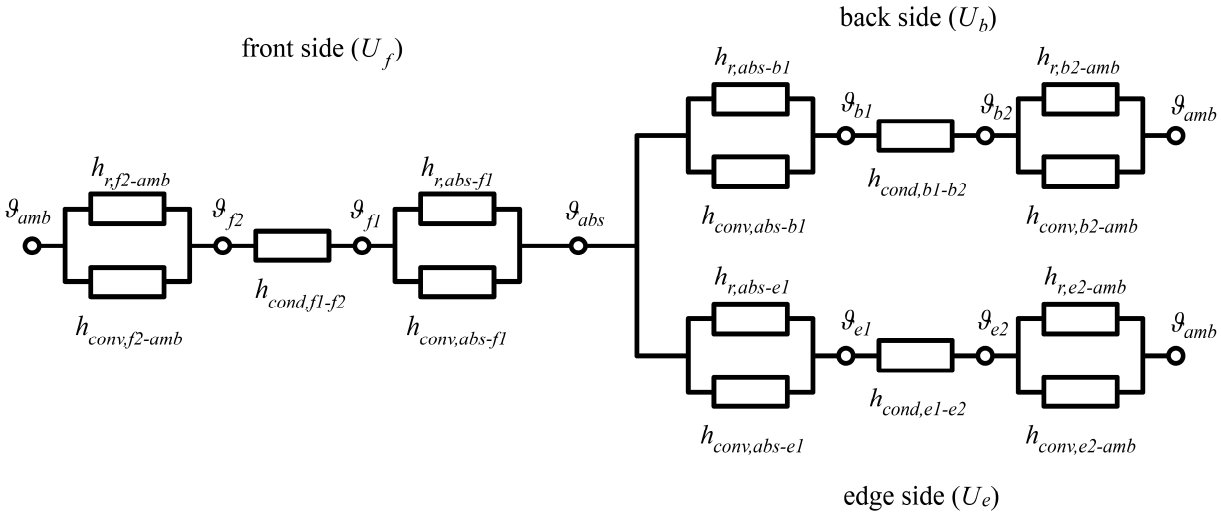

Fig. 2 – Schematic detailed layout of external energy balance of absorber and simplified scheme

6.1.1 Radiation between glazing and sky ($h_{r,f2\text{-}amb}$)

To describe the heat exchange between glazing exterior surface and sky, the sky area is considered as a black body of equivalent temperature ϑ_{sky}. Equivalent sky temperature ϑ_{sky} is introduced due to fact that sky temperature is not uniform and constant and atmosphere radiates only in certain wavelengths ranges in reality.

Radiation heat transfer coefficient is given by

$$h_{r,f2-amb} = \varepsilon_{c2}\sigma \frac{\vartheta_{f2}^4 - \vartheta_{sky}^4}{\vartheta_{f2} - \vartheta_{amb}} \qquad [\mathrm{W/m^2.K}] \tag{5}$$

where

σ is Stefan-Boltzmann constant, $\sigma = 5.67\times10^{-8}$ W/m^2.K^4.

6.1.2 Wind convection from glazing to ambient ($h_{conv,f2\text{-}amb}$)

Heat transfer by convection from exterior surface of collector cover glazing to ambient environment under realistic conditions (mixed natural and forced wind convection) is quite problematic. A large number of relationships and correlations derived from experiments, more or less reproducing the boundary conditions of solar collector installation, can be found in literature (see Tab. 2).

Tab. 2 – Wind convection correlations

M_1	Author	Equation	Range
1	McAdams [7,8]	$h_{conv,f2-amb} = 5.7 + 3.8w$ $h_{conv,f2-amb} = 6.47w^{0.78}$	for $w < 5$ m/s for $w > 5$ m/s
2	Watmuff [9]	$h_{conv,f2-amb} = 2.3 + 3.0w$	$0 < w < 7$ m/s
3	Test [10,11]	$h_{conv,f2-amb} = 8.55 + 2.56w$	$0 < w < 5$ m/s
4	Kumar [12]	$h_{conv,f2-amb} = 10.03 + 4.687w$	$0 < w < 4$ m/s

6.1.3 Conduction through transparent cover ($h_{cond,f1\text{-}f2}$)

For a single cover glazing the conductance can be considered as a constant and calculated as

$$h_{cond,f1-f2} = \frac{\lambda_{gl}}{d_{f1-f2}} \quad [\mathrm{W/m^2.K}] \tag{6}$$

where

λ_{gl} thermal conductivity of cover, W/m.K;

$d_{fl\text{-}f2}$ thickness of cover, m.

In the case of transparent inhomogeneous insulation structures application (e.g. transparent thermal insulations), thermal conductance of the structure should be determined as a function of mean glazing temperature $\vartheta_{f1\text{-}f2}$

$$h_{cond,f1-f2} = f\left(\vartheta_{f1-f2}\right) = f\left(\frac{\vartheta_{f1} + \vartheta_{f2}}{2}\right) = h_{cov0} + h_{cov1}\vartheta_{f1-f2} + h_{cov2}\vartheta^2_{f1-f2} \quad [\mathrm{W/m^2.K}] \tag{7}$$

6.1.4 Natural convection in closed gas layer between absorber and glazing ($h_{conv,abs\text{-}f1}$)

Heat transfer by natural convection in the closed gas layer between absorber and glazing is characterized by Nusselt number Nu_d related to characteristic dimension of the layer, the thickness d_f. Geometric parameters of the gas layer and heat flow direction (upward) are outlined in Fig. 3.

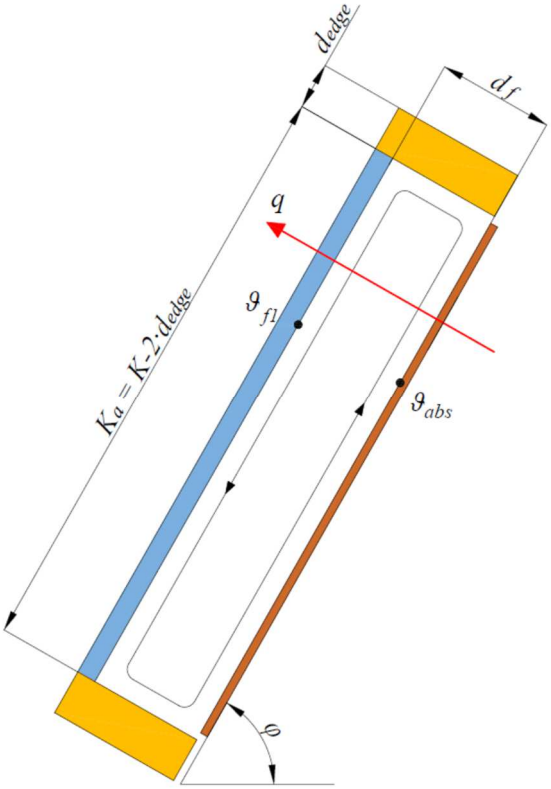

Fig. 3 – Natural convection in closed gas layer (heat flow upward)

Natural convection heat transfer coefficient for closed inclined layer between absorber and cover glazing can be obtained from

$$h_{c,abs-fl} = \frac{\mathrm{Nu}_d \lambda_g}{d_f} \quad [\mathrm{W/m^2.K}] \tag{8}$$

where

λ_g is thermal conductivity of still gas for mean temperature $\vartheta_{abs\text{-}fl}$ in the gas layer, W/m.K.

Nusselt number for natural convection is dependent on Rayleigh number Ra_d, i.e. product of Grashof number Gr_d and Prandtl number Pr.

$$\mathrm{Ra}_d = \mathrm{Gr}_d \,\mathrm{Pr} \quad [-] \tag{9}$$

Prandtl number can be obtained from the properties of used gas at mean temperature of the layer $\vartheta_{abs\text{-}fl}$ as given

$$\mathrm{Pr} = \frac{\nu \rho c}{\lambda} \quad [-] \tag{10}$$

where

ν is kinematic viscosity of gas, $\mathrm{m^2/s}$;

ρ density of gas, $\mathrm{kg/m^3}$;

c specific thermal capacity of gas, J/kg.K.

Grashof number Gr_d is given by

$$Gr_d = \frac{\beta g L^3 \Delta\vartheta}{\nu^2} = \frac{1}{\vartheta_{abs-f1}} \frac{g d_{f1}^3 \left(\vartheta_{abs} - \vartheta_{f1}\right)}{\nu^2} \quad [-] \tag{11}$$

where

β is volumetric thermal expansion coefficient, 1/K;

g gravity acceleration, m/s^2.

Number of published experiments and derived correlations has been found for natural convection heat transfer in sloped enclosure.

Tab. 3 – Selected correlations for natural convection Nusselt number in the sloped closed gas layer (heat flow upward)

M_2	Author	Equation	Range		
			Ra_d	φ	K_a/d_f
1	Hollands [13]	$Nu_d = 1 + 1.44\left[1 - \frac{1708}{Ra_d \cos\varphi}\right]^+ \left(1 - \frac{(\sin\varphi)^{1.6} 1708}{Ra_d \cos\varphi}\right) + \left[\left(\frac{Ra_d \cos\varphi}{5830}\right)^{1/3} - 1\right]^+$	$0 < Ra_d < 10^5$	0°-60°	cca 48
2	Buchberg [14]	for 3 ranges $Nu_d = 1 + 1.44\left[1 - \frac{1708}{Ra_d \cos\varphi}\right]^+$ $Nu_d = 0.229(Ra_d \cos\varphi)^{0.252}$ $Nu_d = 0.157(Ra_d \cos\varphi)^{0.285}$	$1708 < Ra_d\cos\varphi < 10^5$ $5900 < Ra_d\cos\varphi < 9.2\text{x}10^4$ $9.2\text{x}10^4 < Ra_d\cos\varphi < 10^6$	0°-60°	
3	Randal [15]	$Nu_d = 0.118\left[Ra_d \cos^2(\varphi - 45)\right]^{0.29}$	$2.8\text{x}10^3 < Ra_d\cos\varphi < 2.2\text{x}10^5$	45°-90°	9-36
4	Schinkel [16]	$Nu_d = a(\varphi) Ra_d^{1/3}$ φ / $a(\varphi)$: 0° 0.080; 10° 0.079; 20° 0.075; 30° 0.074; 40° 0.074; 50° 0.074; 60° 0.072; 70° 0.069; 80° 0.068; 90° 0.062	$10^5 < Ra_d\cos\varphi < 4\text{x}10^6$	0°-90°	6-27
5	Niemann [17]	$Nu_d = 1 + \frac{m(Ra_d)^c}{Ra_d + n}$ φ / m / n / c: 0° 0.0700 / $0.32\text{x}10^4$ / 1.333; 45° 0.0430 / $0.41\text{x}10^4$ / 1.360; 90° 0.0236 / $1.01\text{x}10^4$ / 1.393	$10^2 < Ra_d < 10^8$		
6	Matuška [5]	$Nu_d = \left(0.1464 - 2.602\times10^{-4}\varphi - 2.046\times10^{-6}\varphi^2\right) Ra_d^{0.29}$	integral correlation (see [5])		

superscript + indicates that content of brackets is considered only for positive values, for negative values the content is equal to 0.

6.1.5 Radiation between absorber and cover glazing ($h_{r,abs-f1}$)

Radiation heat transfer coefficient for heat transfer between absorber and cover glazing can be obtained from

$$h_{r,abs-f1} = \frac{\sigma}{\frac{1}{\varepsilon_{abs,f}} + \frac{1}{\varepsilon_{c1}} - 1} \frac{\vartheta_{abs}^4 - \vartheta_{f1}^4}{\vartheta_{abs} - \vartheta_{f1}} \quad [\mathrm{W/m^2.K}] \tag{12}$$

6.1.6 Natural convection between absorber and back insulation ($h_{conv,abs-b1}$)

Natural convection heat transfer coefficient in enclosed gas layer between absorber and insulation is given by similar equation as in 6.1.4. Geometric parameters of gas layer and heat flow direction (downward) are outlined in Fig. 4.

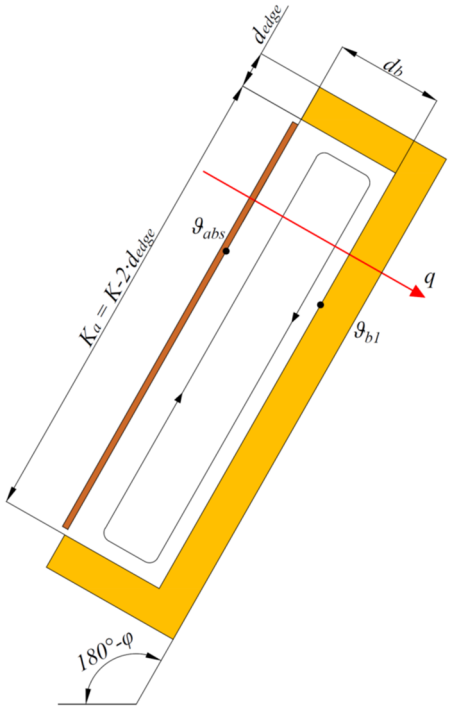

Fig. 4 – Natural convection in closed gas layer (heat flow downward)

$$h_{c,abs-b1} = \frac{\mathrm{Nu}_d \lambda_g}{d_b} \quad [\mathrm{W/m^2.K}] \tag{13}$$

where

λ_g is thermal conductivity of still gas for mean temperature ϑ_{abs-b1} in the gas layer, W/m.K.

A literature review has been done to find proper equation for heat transfer coefficient for the case of natural convection in gas enclosure (closed gas layer) with heat flow downward required. Only one general equation has been obtained. Arnold et al. [18] suggest correlation based on Nusselt number obtained for vertical gas layer (90°) as a sinus function in the range of 90-180° as given

$$\mathrm{Nu}_d = 1 + \left[\mathrm{Nu}_d(\varphi = 90^\circ) - 1\right] \sin(180^\circ - \varphi) \quad [-] \tag{14}$$

6.1.7 Radiation between absorber and back insulation ($h_{r,abs-b1}$)

Radiation heat transfer coefficient between back surface of absorber and back insulation is given by Stefan-Boltzman law similarly as in chapter 6.1.5

$$h_{r,abs-b1} = \frac{\sigma}{\frac{1}{\varepsilon_{abs,b}} + \frac{1}{\varepsilon_{ins}} - 1} \frac{\vartheta_{abs}^4 - \vartheta_{b1}^4}{\vartheta_{abs} - \vartheta_{b1}} \quad [\mathrm{W/m^2.K}] \qquad (15)$$

Distinction between front and back absorber surface emittance is necessary since most of solar flat-plate collectors is equipped with spectrally selective coating at front absorber surface (low emittance in IR region) while back surface is left without any treatment (oxidized, dirty, etc.).

6.1.8 Conduction heat transfer through insulation ($h_{cond,b1-b2}$)

The thermal conductivity of the insulation depends on the mean temperature of insulation. Therefore, there should be a relationship between the thermal conductivity and mean temperature. This relation is non-linear and is different both for different insulation materials and for different manufacturers of insulation materials (Fig. 5).

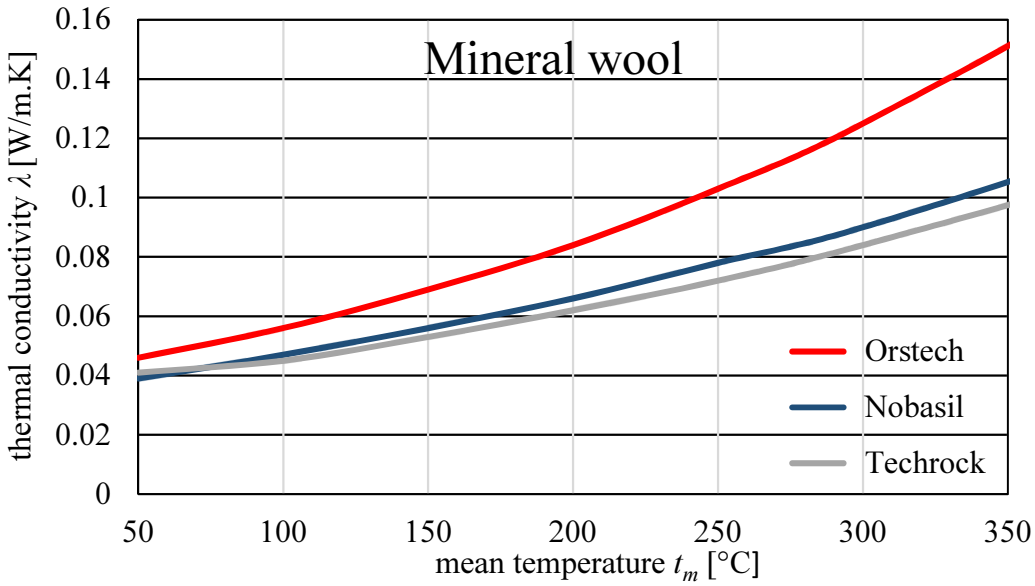

Fig. 5 – Thermal conductivity as a function of mean temperature of insulation

It obeys a polynomial function:

$$\lambda = \lambda(\vartheta_{b1-b2}) = f\left(\frac{\vartheta_{b1} + \vartheta_{b2}}{2}\right) = \lambda_0 + \lambda_1 \vartheta_{b1-b2} + \lambda_2 \vartheta_{b1-b2}^2 \quad [\mathrm{W/m.K}] \qquad (16)$$

Therefore heat transfer coefficient have to be determined as a function of the mean temperature of the insulation ϑ_{b1-b2}.

$$h_{cond,b1-b2} = \frac{\lambda}{d_{ins}} = \frac{\lambda(\vartheta_{b1-b2})}{d_{ins}} = \frac{\lambda_0}{d_{ins}} + \frac{\lambda_1}{d_{ins}} \vartheta_{b1-b2} + \frac{\lambda_2}{d_{ins}} \vartheta_{b1-b2}^2 = h_{ins0} + h_{ins1} \vartheta_{b1-b2} + h_{ins2} \vartheta_{b1-b2}^2 \quad [\mathrm{W/m^2.K}] \qquad (17)$$

6.1.9 Radiation heat exchange between frame and adjacent ambient surfaces ($h_{r,b2\text{-}amb}$)

Radiation heat transfer coefficient between exterior surface of collector back frame and adjacent surfaces in ambient environment (roof) related to ambient temperature ϑ_{amb} can be expressed as

$$h_{r,b2-amb} = \frac{\sigma}{\frac{1}{\varepsilon_{fs}} + \frac{1}{\varepsilon_{as}} - 1} \frac{\vartheta_{b2}^4 - \vartheta_{amb}^4}{\vartheta_{b2} - \vartheta_{amb}} \text{ [W/m}^2\text{.K]} \quad (18)$$

6.1.10 Wind convection heat transfer from back frame to ambient ($h_{conv,b2\text{-}amb}$)

Wind convection heat transfer coefficient from back side of collector frame to ambient can be determined identically as in 6.1.2.

6.1.11 Radiation and convection heat exchange between absorber and edge insulation ($h_{r,abs\text{-}e1}$ and $h_{conv,abs\text{-}e1}$)

The estimation of edge losses is complicated for most collectors. However the edge losses are small for a standard size of collector box and it is not necessary to predict them with great accuracy. According to Duffie and Beckman [5] the magnitudes of the thermal resistance of convection and radiation heat transfer between absorber and edge insulation are much smaller than that of conduction through edge insulation and heat transfer from the edge frame of the collector to surroundings. Therefore it can be assumed that the temperature of edge insulation ϑ_{e1} is equal to absorber temperature ϑ_{abs}.

6.1.12 Conduction heat transfer through insulation ($h_{cond,e1\text{-}e2}$)

Thermal conductance of the edge insulation can be determined identically as in 6.1.8.

6.1.13 Wind convection heat transfer from edge frame to ambient ($h_{conv,e2\text{-}amb}$)

Wind convection heat transfer coefficient from edge side of collector frame to ambient can be determined identically as in 6.1.2.

6.1.14 Radiation heat exchange between edge frame and adjacent surfaces ($h_{r,e2\text{-}amb}$)

Radiation heat transfer coefficient between exterior surface of collector edge frame and adjacent surfaces in ambient environment (roof) can be determined identically as in 6.1.9.

6.1.15 Collector heat loss coefficient (U-value)

As illustrated in Fig. 2 heat loss coefficient for front side of the collector U_f can be determined as

$$U_f = \frac{1}{\frac{1}{h_{r,f2-amb} + h_{conv,f2-amb}} + \frac{1}{h_{cond,f1-f2}} + \frac{1}{h_{r,abs-f1} + h_{conv,abs-f1}}} \text{ [W/m}^2\text{.K]} \quad (19)$$

By analogy, heat loss coefficient for back side U_b and for edge side U_e of the collector can be determined as

$$U_b = \frac{1}{\frac{1}{h_{r,b2-amb} + h_{conv,b2-amb}} + \frac{1}{h_{cond,b1-b2}} + \frac{1}{h_{r,abs-b1} + h_{conv,abs-b1}}} \quad [\mathrm{W/m^2.K}] \tag{20}$$

$$U_e = \frac{1}{\frac{1}{h_{r,e2-amb} + h_{conv,e2-amb}} + \frac{1}{h_{cond,e1-e2}}} \quad [\mathrm{W/m^2.K}] \tag{21}$$

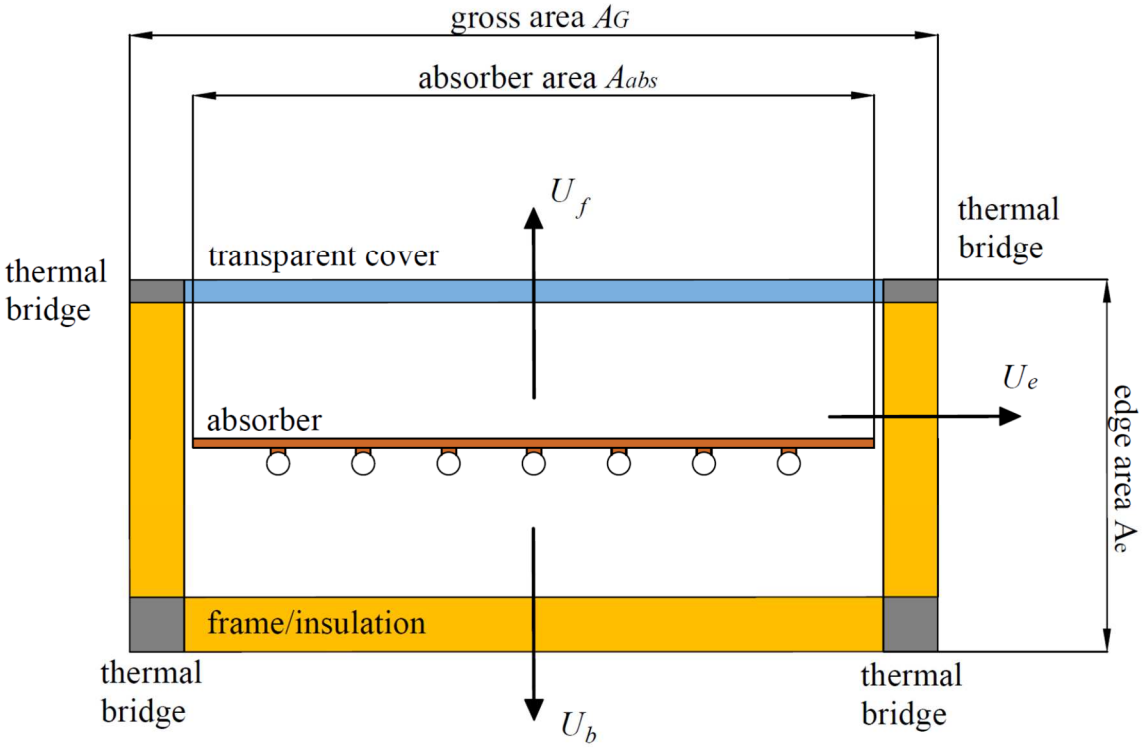

Fig. 6 – Collector heat loss with respect to aperture and gross area

Overall heat loss of solar collector (U-value) is related to gross dimensions (gross collector area A_G) as illustrated in Fig. 6 to cover the effect of thermal bridges not to underestimate the heat loss. On the other side, the usable heat output of the collector refers to absorber area A_{abs}, therefore overall collector heat loss coefficient U used in the internal energy balance calculations should be also related to absorber area A_{abs}.

The overall heat loss coefficient U based on absorber area can be obtain as

$$U = \left(U_f + U_b + U_e \frac{A_e}{A_G} \right) \frac{A_G}{A_{abs}} \quad [\mathrm{W/m^2.K}] \tag{22}$$

6.1.16 Recalculation of surface temperatures

Since heat transfer and heat loss coefficients have been calculated for incorrect temperatures (first estimates), next iteration step should follow. From heat transfer coefficients and heat flows through front, back and edge side of the solar collector the temperature distribution can be obtained by reverse calculation process as follows

$$\vartheta_{f1} = \vartheta_{abs} - \frac{U_f\left(\vartheta_{abs} - \vartheta_{amb}\right)}{h_{r,abs-f1} + h_{conv,abs-f1}} \quad [\mathrm{K}] \tag{23}$$

$$\vartheta_{f2} = \vartheta_{amb} + \frac{U_f\left(\vartheta_{abs} - \vartheta_{amb}\right)}{h_{r,f2-amb} + h_{conv,f2-amb}} \quad [\mathrm{K}] \tag{24}$$

Analogous to front side surface temperatures calculation, for back side and edge side can be applied

$$\vartheta_{b1} = \vartheta_{abs} - \frac{U_b\left(\vartheta_{abs} - \vartheta_{amb}\right)}{h_{r,abs-b1} + h_{conv,abs-b1}} \quad [\mathrm{K}] \tag{25}$$

$$\vartheta_{b2} = \vartheta_{amb} + \frac{U_b\left(\vartheta_{abs} - \vartheta_{amb}\right)}{h_{r,b2-amb} + h_{conv,b2-amb}} \quad [\mathrm{K}] \tag{26}$$

$$\vartheta_{e1} = \vartheta_{abs} \quad [\mathrm{K}] \tag{27}$$

$$\vartheta_{e2} = \vartheta_{amb} + \frac{U_e\left(\vartheta_{abs} - \vartheta_{amb}\right)}{h_{r,e2-amb} + h_{conv,e2-amb}} \quad [\mathrm{K}] \tag{28}$$

The new and more correct values of surface temperatures are used in next iteration step for calculation of individual heat transfer coefficients between the surfaces and new and more correct value of heat loss coefficient U (see Fig. 2).

6.2 Internal energy balance

The internal energy balance considers:

- fin and tube absorber (M_6 = 1 - 3);
  1) fin heat transfer by conduction;
  2) heat transfer by conduction through the bond between absorber and pipes;
  3) heat transfer by forced convection from interior surface of pipe to fluid;
- fully wetted absorber (M_6 = 4);
  1) heat transfer by forced convection from the absorber surface to fluid.

Internal energy balance proceeds in its own iteration loop with respect to relative dependence between mean fluid temperature ϑ_{mean} and forced convection heat transfer coefficients in absorber pipe register.

In the first iteration cycle of internal energy balance, the mean fluid temperature is estimated from ϑ_{in} by relationship:

$$\vartheta_{mean} = \vartheta_{in} + 10 \qquad [\mathrm{K}] \qquad (29)$$

With use of this first estimate of mean fluid temperature ϑ_{mean} the collector efficiency factor F', collector heat removal factor F_R, usable thermal power and efficiency of solar collector can be calculated.

6.2.1 Fin efficiency F (M_6 = 1 - 3)

When considered absorber element as a fin, it is convenient to introduce the concept of fin efficiency given by

$$F = \frac{\tanh\left[m(W-2a)/2\right]}{m(W-2a)/2} \qquad [-] \qquad (30)$$

where

$$m = \sqrt{\frac{U}{\lambda_{abs} d_{abs}}} \qquad [-] \qquad (31)$$

6.2.2 Collector efficiency factor F'

Except the conduction heat transfer by the fin (M_6 = 1 - 3), also conduction through the bond fin-pipe (M_6 = 1 - 3) and heat transfer from pipe to liquid by forced convection influence the overall heat transfer from absorber surface to heat transfer liquid. Collector or absorber efficiency factor F' is introduced to describe how "efficient" the heat transfer from absorber surface to heat transfer fluid is.

Different absorber configurations (see Fig. 7-10) result in appropriate equations. For the most used upper bond of absorber to riser pipes (M_6 = 1) the efficiency factor is given as

$$F' = \frac{1/U}{W\left[\frac{1}{U\left[2a+(W-2a)F\right]} + \frac{1}{C_b} + \frac{1}{h_i \pi D_i}\right]} \qquad [-] \qquad (32)$$

where

h_i is forced convection heat transfer coefficient in riser pipe, W/m^{2}K.

and bond thermal conductance C_b is calculated from

$$C_b = \frac{\lambda_b a}{b} \qquad [\mathrm{W/m.K}] \qquad (33)$$

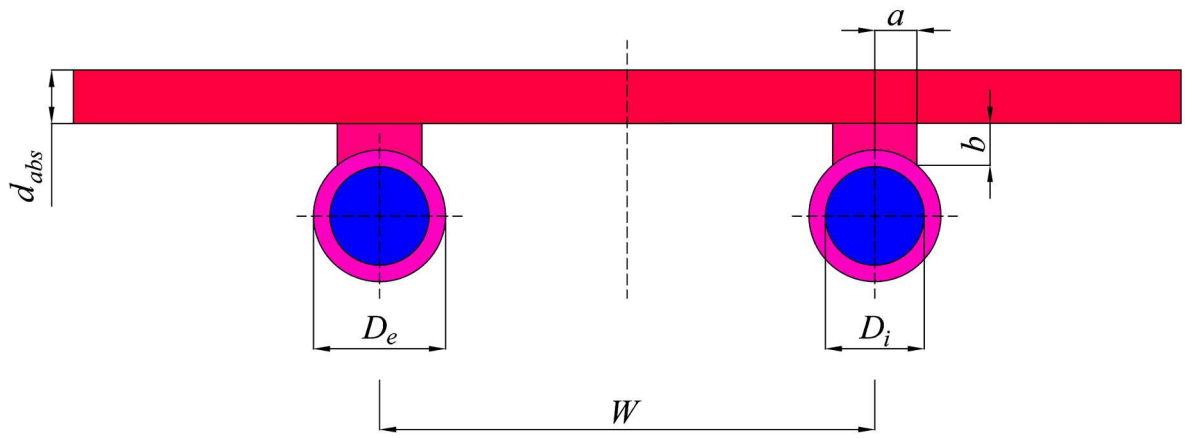

Fig.7 – Absorber-pipe upper bond configuration

For side bond of absorber to riser pipes ($M_5 = 2$) the efficiency factor is given as

$$F' = \frac{1/U}{W\left[\frac{1}{U\left[D_e + (W - D_e)F\right]} + \frac{1}{h_i \pi D_i}\right]} \quad [-] \qquad (34)$$

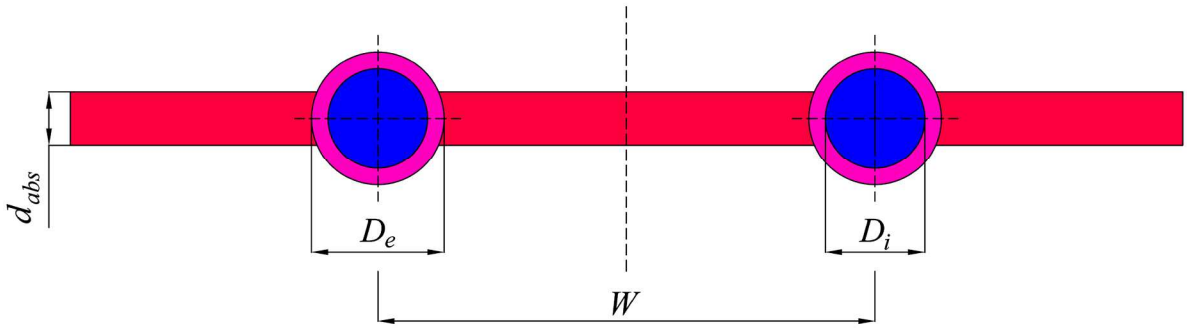

Fig. 8 – Absorber–pipe side bond configuration

For lower bond of absorber to riser pipes ($M_5 = 3$) the efficiency factor is given as

$$F' = \frac{1/U}{\frac{WU}{h_i \pi D_i} + \frac{1}{\frac{2a}{W} + \frac{1}{\frac{WU}{C_b} + \frac{W}{(W - 2a)F}}}} \quad [-] \qquad (35)$$

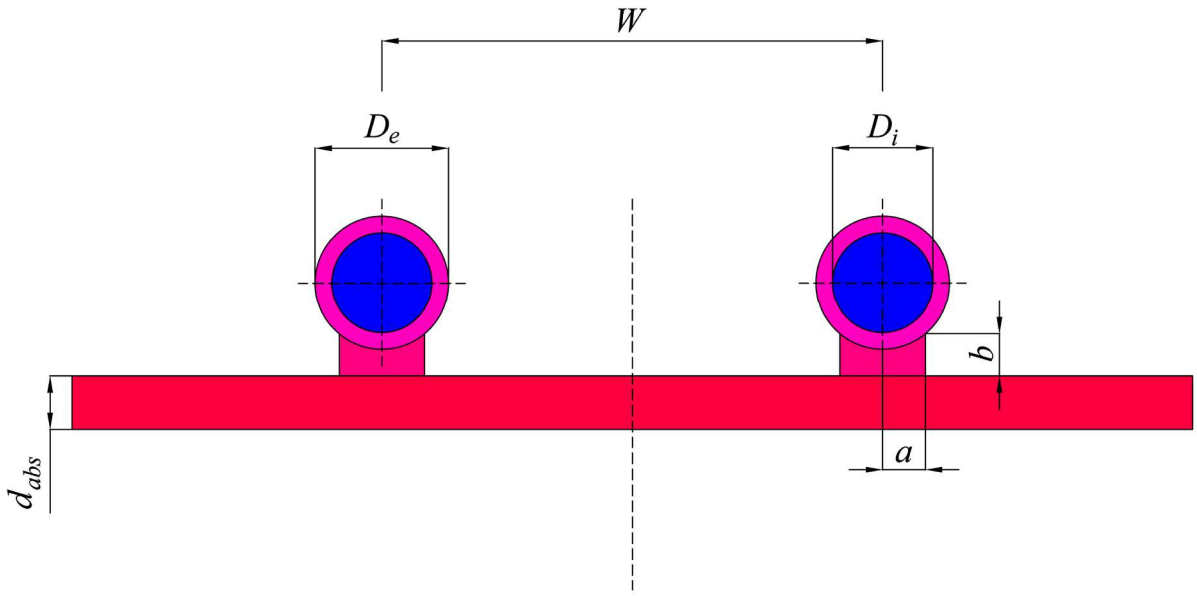

Fig. 9 – Absorber–pipe lower bond configuration

For the case of fully wetted absorber (M_5 = 4) the efficiency factor is given as

$$F' = \frac{h_i}{h_i + U\left(\frac{h_i d_{abs}}{\lambda_{abs}} + 1\right)} \qquad [-] \qquad (36)$$

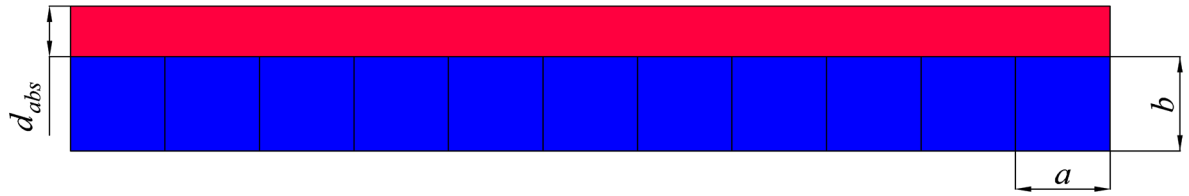

Fig. 10 – Fully wetted configuration

6.2.3 Forced convection heat transfer in pipes (h_i)

Forced convection heat transfer coefficient between the fluid and wall in absorber riser pipe (M_5 = 1 - 3) or between the fluid and absorber surface (M_5 = 4) is determined from Nusselt number

$$h_i = \mathrm{Nu}_D \frac{\lambda_f}{D_i} \qquad [\mathrm{W/m^2K}] \qquad (37)$$

where

λ_f is thermal conductivity of heat transfer fluid, W/m.K.

In the case of fully wetted absorber configuration, an effective diameter should be used as the characteristic length and it is defined as

$$D_i = \frac{4ab}{2(a+b)} \qquad [\mathrm{m}] \qquad (38)$$

Laminar forced convection heat transfer in circular pipes is widely described in literature. Tab. 4 shows correlations for Nusselt number for laminar forced convection heat transfer found in literature. In the case of developing flow, dimensionless longitudinal coordinate x^* is defined as inverse value of Graetz number characterizing the laminar flow in pipes as given in equation

$$x^* = \mathrm{Gz}^{-1} = \frac{L/D_i}{\mathrm{Re}_D \,\mathrm{Pr}} \quad [-] \tag{39}$$

Tab. 4 – Correlations for laminar forced convection heat transfer in pipes

M_6	Author	Equation	Conditions
1	Shah [19]	$\mathrm{Nu}_D = 4.364$	fully developed velocity and temperature profile, constant heat flux
2	Shah [19]	$\mathrm{Nu}_D = 1.953 x^{*-1/3}$ $\quad x^* \le 0.03$ $\mathrm{Nu}_D = 4.364 + \frac{0.0722}{x^*}$ $\quad x^* > 0.03$	entry region of length L, developing profile, constant heat flux
3	Hausen [20]	$\mathrm{Nu}_D = 3.66 + \frac{0.668(D/L)\mathrm{Re}_D \,\mathrm{Pr}}{1+0.04[(D/L)\mathrm{Re}_D \,\mathrm{Pr}]^{2/3}}$	entry region of length L, developing profile
4	Sieder-Tate [21]	$\mathrm{Nu}_D = 1.86\left(\frac{1}{x^*}\right)^{1/3}\left(\frac{\mu}{\mu_w}\right)$	entry region - thermally and hydraulically developing flow $0.48 < \mathrm{Pr} < 16700$ $0.0044 < \left(\frac{\mu}{\mu_w}\right) < 9.75$ recommended for $\left(\frac{1}{x^*}\right)^{1/3}\left(\frac{\mu}{\mu_w}\right)^{0.14} > 2$ else fully developer profile
5	Churchill and Ozoe [22]	$\mathrm{Nu}_D = \frac{2 \cdot 0.6366[(4/\pi)x*]^{-1/2}}{\left[1+(\mathrm{Pr}/0.0468)^{2/3}\right]^{1/4}}$	entry region - thermally and hydraulically developing flow $\mathrm{Pr} > 2$ $10^{-7} < \mathrm{x} < 10^{-3}$

In the case of turbulent flow, different set of equations (see Tab. 5) is applicable to calculation of the Nusselt number, mostly in the form

$$\mathrm{Nu}_D = A\,\mathrm{Re}_D^m \,\mathrm{Pr}^n \quad [-] \tag{40}$$

The turbulent flow inside the riser pipes of solar collectors is very rare when using antifreeze water-glycol mixtures as heat transfer fluid with high viscosity.

Tab. 5 – Correlations for laminar forced convection heat transfer in pipes

M_7	Author	Equation	Conditions
1	Colburn [23]	$\mathrm{Nu}_D = 0.023\,\mathrm{Re}_D^{4/5}\,\mathrm{Pr}^{1/3}$	$2\text{x}10^4 < \mathrm{Re}_D < 10^6$
2	Dittus-Boelter [24]	$\mathrm{Nu}_D = 0.023\,\mathrm{Re}_D^{4/5}\,\mathrm{Pr}^{0.4}$ for heating $\mathrm{Nu}_D = 0.023\,\mathrm{Re}_D^{4/5}\,\mathrm{Pr}^{0.3}$ for cooling	$0.7 < \mathrm{Pr} < 120$ $2500 < \mathrm{Re}_D < 1.24\text{x}10^5$ $L/D > 60$
3	Kakac [25]	$\mathrm{Nu}_D = 0.023\,\mathrm{Re}_D^{4/5}\,\mathrm{Pr}^{0.4}$ for heating $\mathrm{Nu}_D = 0.026\,\mathrm{Re}_D^{4/5}\,\mathrm{Pr}^{0.4}$ for cooling	
4	Petukhov-Kirillov-Popov [26]	$\mathrm{Nu}_D = \frac{(f/8)\mathrm{Re}_D\,\mathrm{Pr}}{1.07+12.7(f/8)^{1/2}\left(\mathrm{Pr}^{2/3}-1\right)}$ friction factor according Moody diagram smoth pipes $f = (1.82\log_{10}\mathrm{Re}_D - 1.64)^{-2}$	$0.5 < \mathrm{Pr} < 2000$ $10^4 < \mathrm{Re}_D < 5\text{x}10^6$
5	Gnielinski [27]	$\mathrm{Nu}_D = \frac{(f/8)(\mathrm{Re}_D-1000)\mathrm{Pr}}{1+12.7(f/8)^{1/2}\left(\mathrm{Pr}^{2/3}-1\right)}$ friction factor according Moody diagram smoth pipes $f = (0.79\ln\mathrm{Re}_D - 1.64)^{-2}$	$0.5 < \mathrm{Pr} < 2000$ $10^4 < \mathrm{Re}_D < 5\text{x}10^6$
6	Sleicher, Rouse [28]	$\mathrm{Nu}_D = 5 + 0.015\,\mathrm{Re}_D^a\,\mathrm{Pr}^b$ $a = 0.88 - \frac{0.24}{4+\mathrm{Pr}}$ $b = 0.333 + 0.5e^{-0.6\mathrm{Pr}}$	$0.1 < \mathrm{Pr} < 10^4$ $10^4 < \mathrm{Re}_D < 10^6$

6.2.4 Collector heat removal factor F_R

It is convenient to define a quantity that relates the actual useful energy gain of a collector to the useful gain if the whole collector surface were at the fluid inlet temperature. This quantity is called the collector heat removal factor F_R. In equation form it is

$$F_R = \frac{\dot{m}c_f}{A_{abs}U}\left[1-\exp\left(-\frac{A_{abs}UF'}{\dot{m}c_f}\right)\right] \text{ [-]} \qquad (41)$$

where

c_f is specific thermal capacity of fluid, J/kg.K;

$\dot{m}$ total mass flow rate of fluid through solar collector, kg/s.

Collector heat removal factor F_R is equivalent to the effectiveness of a conventional heat exchanger, which is defined as ratio of the actual heat transfer to the maximum possible heat transfer. Maximum possible useful heat gain in a solar collector occurs when the whole absorber is at the inlet fluid temperature (no temperature increase along the riser pipes, minimized heat loss).

6.2.5 Incident angle modifier K_{net}

The collector absorbs only a portion of the solar irradiance due to the optical properties of the transparent cover and absorber plate, which are described in the $\tau_n\alpha_{abs}$ and the *IAM* parameters for each irradiance component (K_{beam}, K_{sky}, K_{gnd}). Incident angle modifiers are calculated separately for beam (G_{beam}), sky (G_{sky}) and ground radiation (G_{gnd}). The net incident angle modifier for all incident radiation is calculated by weighting each component by the corresponding modifier.

$$K_{net} = \frac{G_{beam}K_{beam} + G_{sky}K_{sky} + G_{gnd}K_{gnd}}{G_t} \quad [-] \tag{42}$$

where

G_t total radiation for collector surface, W/m^2.

$$G_t = G_{beam} + G_{sky} + G_{gnd} \quad [\mathrm{W/m^2}] \tag{43}$$

Incidence angle modifier of solar collector for beam radiation component can be determined by experiment an empirical expression for K_{beam}.

$$K_{beam} = 1 - b_0\left(\frac{1}{\cos\theta} - 1\right) - b_1\left(\frac{1}{\cos\theta} - 1\right)^2 \quad [-] \tag{44}$$

Sky and ground reflected radiation are considered as diffuse isotropic, that means optical properties for this solar radiation components are not considered as incidence angle dependent like for beam radiation but constant. Incidence angle modifier of solar collector for sky and ground radiation components can be approximated using Brandemuehl and Beckman's equations [29] from the K_{beam} characteristic for given effective incident angle:

$$\theta_{eff,sky} = 59.68 - 0.1388\varphi + 0.001497\varphi^2 \quad [°] \tag{45}$$

$$\theta_{eff,gnd} = 90 - 0.5788\varphi + 0.002693\varphi^2 \quad [°] \tag{46}$$

Finally incident angle modifiers for sky-diffuse and ground-reflected radiation are:

$$K_{sky} = 1 - b_0\left(\frac{1}{\cos\theta_{eff,sky}} - 1\right) - b_1\left(\frac{1}{\cos\theta_{eff,sky}} - 1\right)^2 \quad [-] \tag{47}$$

$$K_{gnd} = 1 - b_0\left(\frac{1}{\cos\theta_{eff,gnd}} - 1\right) - b_1\left(\frac{1}{\cos\theta_{eff,gnd}} - 1\right)^2 \quad [-] \tag{48}$$

In the case of $b_1 = 0$, incident angle modifiers for beam, sky and ground radiation have to be calculated by another equations:

$$K_{beam} = 1 - b_0\left(\frac{1}{\max(0.5, \cos\theta)} - 1\right) - \frac{(1 - b_0)(\max(60, \theta) - 60)}{30} \quad [-] \tag{49}$$

$$K_{sky} = 1 - b_0\left(\frac{1}{\max\left(0.5, \cos\theta_{eff,sky}\right)} - 1\right) - \frac{(1-b_0)\left(\max\left(60, \theta_{eff,sky}\right) - 60\right)}{30} \quad [-] \quad (50)$$

$$K_{gnd} = 1 - b_0\left(\frac{1}{\max\left(0.5, \cos\theta_{eff,gnd}\right)} - 1\right) - \frac{(1-b_0)\left(\max\left(60, \theta_{eff,gnd}\right) - 60\right)}{30} \quad [-] \quad (51)$$

6.2.6 Useful heat output of solar collector Q_u

Useful thermal output from solar collector can be defined in three different ways, based on absorber temperature, mean temperature and input temperature.

$$\dot{Q}_u = A_{abs}\left[\tau_n \alpha_{abs} G_t K_{net} - U\left(\vartheta_{abs} - \vartheta_{amb}\right)\right] \quad [W] \quad (52)$$

$$\dot{Q}_u = A_{abs} F'\left[\tau_n \alpha_{abs} G_t K_{net} - U\left(\vartheta_m - \vartheta_{amb}\right)\right] \quad [W] \quad (53)$$

$$\dot{Q}_u = A_{abs} F_R\left[\tau_n \alpha_{abs} G_t K_{net} - U\left(\vartheta_{in} - \vartheta_{amb}\right)\right] \quad [W] \quad (54)$$

This Type uses Equation (52) for calculation of useful thermal output.

6.2.7 Efficiency of solar collector η

Collector efficiency is defined as usable thermal power output from the collector related to solar radiation input incident on front part of collector (gross area A_G) [30]. Collector efficiency can be related to:

mean absorber temperature $$\eta_{abs} = \frac{A_{abs}}{A_G}\left[\tau_n \alpha_{abs} - \frac{U\left(\vartheta_{abs} - \vartheta_{amb}\right)}{G_t K_{net}}\right] \quad [-] \quad (55)$$

mean fluid temperature $$\eta_m = F' \frac{A_{abs}}{A_G}\left[\tau_n \alpha_{abs} - \frac{U\left(\vartheta_m - \vartheta_{amb}\right)}{G_t K_{net}}\right] \quad [-] \quad (56)$$

input fluid temperature $$\eta_{in} = F_R \frac{A_{abs}}{A_G}\left[\tau_n \alpha_{abs} - \frac{U\left(\vartheta_{in} - \vartheta_{amb}\right)}{G_t K_{net}}\right] \quad [-] \quad (57)$$

This Type uses Equation (55) for calculation of useful thermal output.

6.2.8 Recalculation of fluid ϑ_{mean} and absorber temperature ϑ_{abs}

Since useful heat output, collector heat removal factor and collector efficiency factor have been calculated for first estimates of temperatures, next iteration step should follow.

To calculate heat transfer coefficients at main surfaces of solar collector and to assess the overall collector heat loss coefficient U (external energy balance) in the next iteration step the absorber temperature should be identified from input temperature

$$\vartheta_{abs} = \vartheta_{in} + \frac{\dot{Q}_u}{F_R U A_{abs}}\left(1 - F_R\right) \qquad [\mathrm{K}] \tag{58}$$

Mean fluid temperature ϑ_{mean} necessary for calculation of convection heat transfer coefficient h_i for fluid in pipes in the next iteration step can be obtained from input temperature

$$\vartheta_{mean} = \vartheta_{in} + \frac{\dot{Q}_u}{F_R U A_{abs}}\left(1 - \frac{F_R}{F'}\right) \qquad [\mathrm{K}] \tag{59}$$

7 Iteration loop

Both external and internal energy balances are mutually dependent. Overall collector heat loss coefficient U as main output from external balance is one of the inputs for internal balance. On the other side, mean absorber temperature ϑ_{abs} as one of the outputs from internal balance is used as necessary input for external balance. Iteration loop has been introduced to transfer the results from external balance to starting internal balance and results from internal balance are put to external balance. Loop iterates as long as the difference between absorber temperatures calculated in two adjacent iteration steps is more than 0.01 K

$$\left|\vartheta_{abs}^{N} - \vartheta_{abs}^{N-1}\right| \geq 0.01 \quad [\mathrm{K}] \tag{60}$$

where

N is iteration counter, [-].

When this condition becomes false, the iteration process stops. Iteration loop generally converges very quickly. The absorber temperature distribution becomes stable and iteration loop is finished after 5-6 iterations.

The scheme of iteration loop is outlined in Fig. 11.

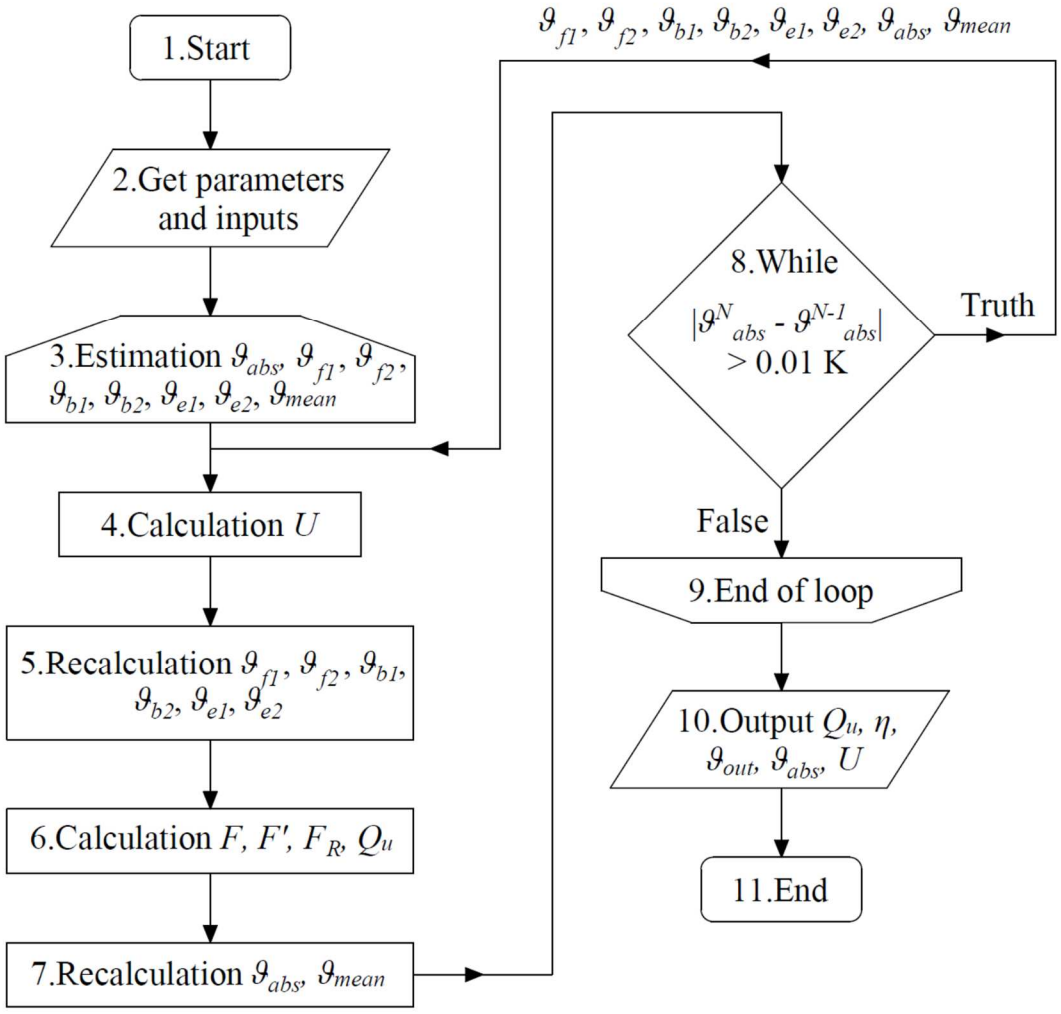

Fig. 11 – Flow chart of the iteration loop

8 Experimental validation

Type 205 has been experimentally validated in the frame of solar collectors testing according to European standard [30] in the Solar Laboratory operated under University Centre for Energy Efficient Buildings, Czech Technical University in Prague accredited under Institute for Testing and Certification, Zlin. Solar thermal collectors have been tested to obtain steady state performance thermal output at constant operation conditions of inlet temperature (±0.05 K) and mass flow rate (±0.002 %) of heat transfer fluid (water) entering collector and at constant climatic conditions of solar irradiation (±1.4 %) and ambient temperature (±0.05 K). Instantaneous efficiency has been calculated from collector thermal output related to total solar irradiation input (incident on collector reference area: gross area). The efficiency curve (dependence of efficiency on mean reduced temperature difference) has been obtained from at least 5 points in the range of input fluid temperature from ambient (around 20 °C) to 90 °C. Experimental data points of solar collector efficiency has been coupled with uniform uncertainty bars in the graphs. Expanded efficiency and reduced temperature difference uncertainties have been assessed for experimental data from both type A (statistical) and type B (instrumental) uncertainties considering the coverage factor 2 with 95% level of confidence

[31, 32]. For usual steady state conditions of measurements the expanded efficiency uncertainty lies between 1.0 and 1.5 %. Expanded reduced temperature difference uncertainty lies between 0.0001 and 0.0014 m^2.K/W.

The theoretical calculation of efficiency curve by model is subjected to uncertainty of input parameters. While geometrical parameters are easily available with high degree of confidence, number of parameters defining the properties of collector parts is found uncertain within narrow range (e.g. absorber and glazing properties parameters, mostly ±2 %), middle range (e.g. conductivity of insulation layer dependent on its temperature and density, ±10 %) and quite broad range (e.g. emittance of absorber back side, insulation or collector frame, > 50 %). Each of varying parameter has a different impact (sensitivity) to resulting efficiency value from high effect of absorber and glazing optical properties to negligible effect of frame external surface emittance. Uncertainty of input parameters and its influence to calculated efficiency has been expressed by two dashed borderlines where the collector efficiency values can be found in reality.

Mathematical model has been validated in the field of atmospheric solar flat-plate collectors (top quality solar collectors with state-of-art copper laser welded absorber coated with high performance selective coating and solar antireflective glazing). Fig. 12 – 15 show validation of the model for four examples of different atmospheric flat-plate collectors. Mathematical model has been also tested in the case of various values of slope, mass flowrate, wind velocity and incident radiation (Fig. 16 – 22).

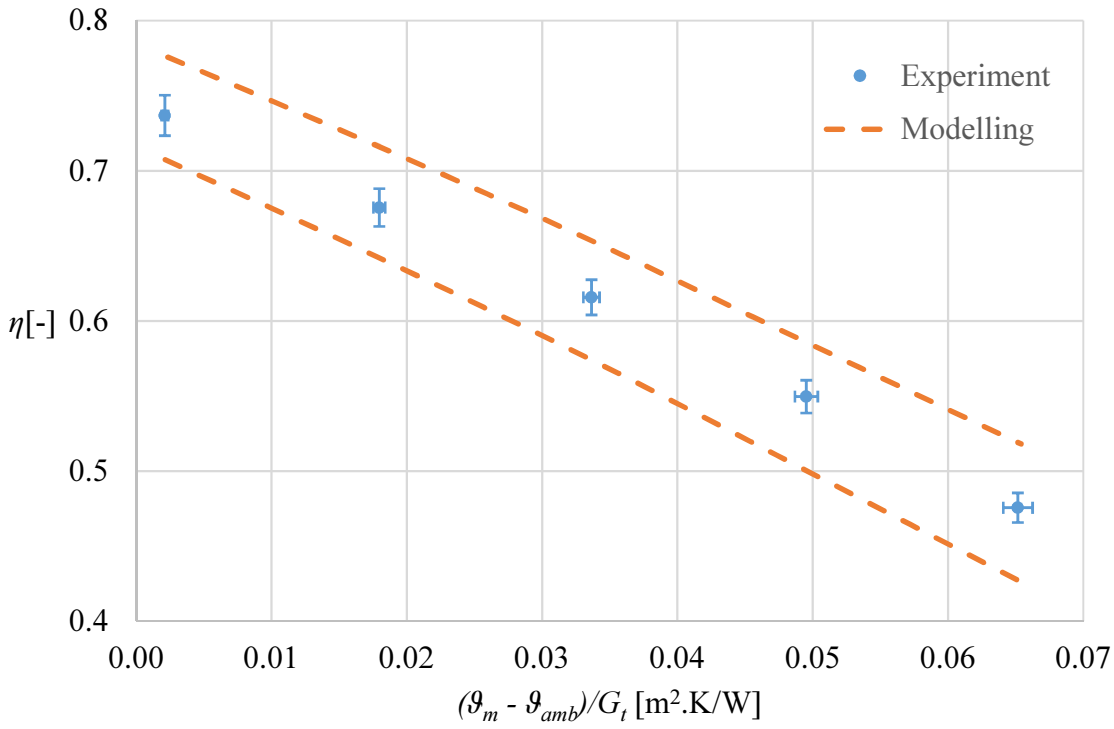

Fig. 12 – Experimental evaluation of the detailed theoretical model by collector testing (flat-plate collector № 1)

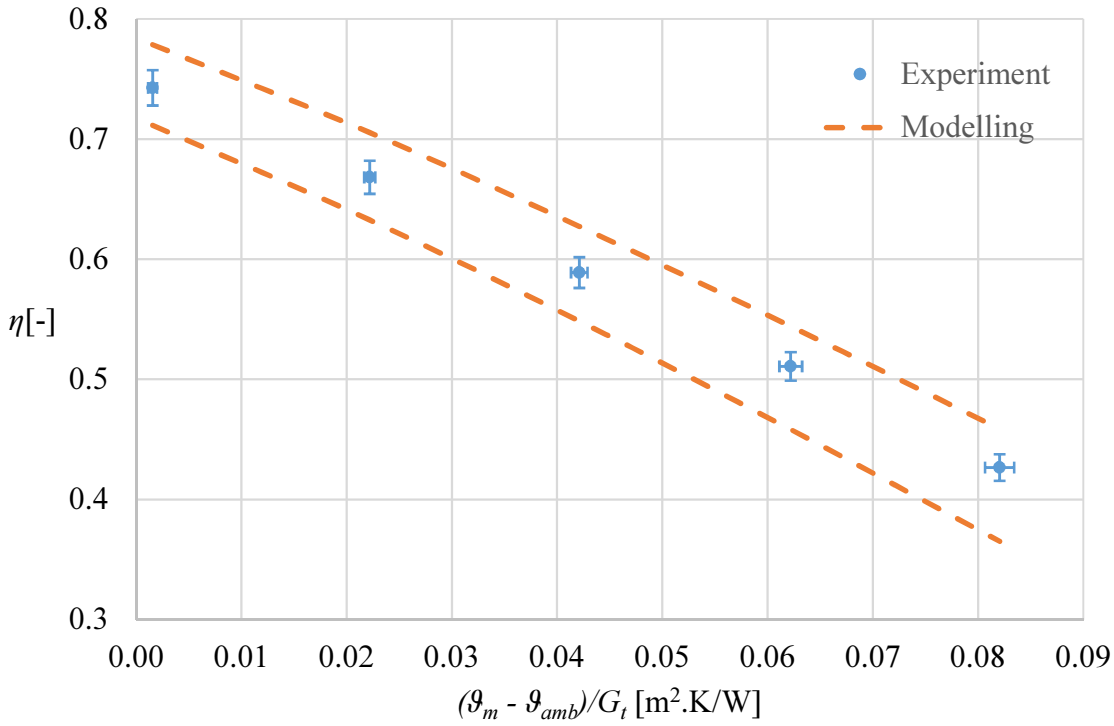

Fig. 13 – Experimental evaluation of the detailed theoretical model by collector testing (flat-plate collector № 2)

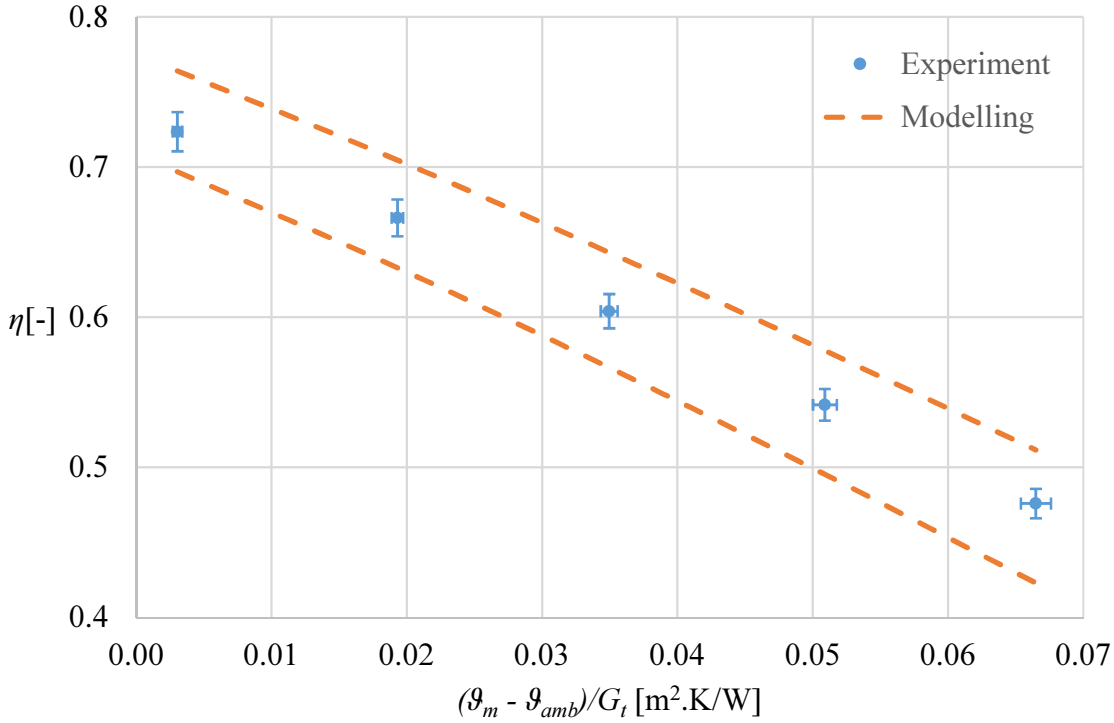

Fig. 14 – Experimental evaluation of the detailed theoretical model by collector testing (flat-plate collector № 3)

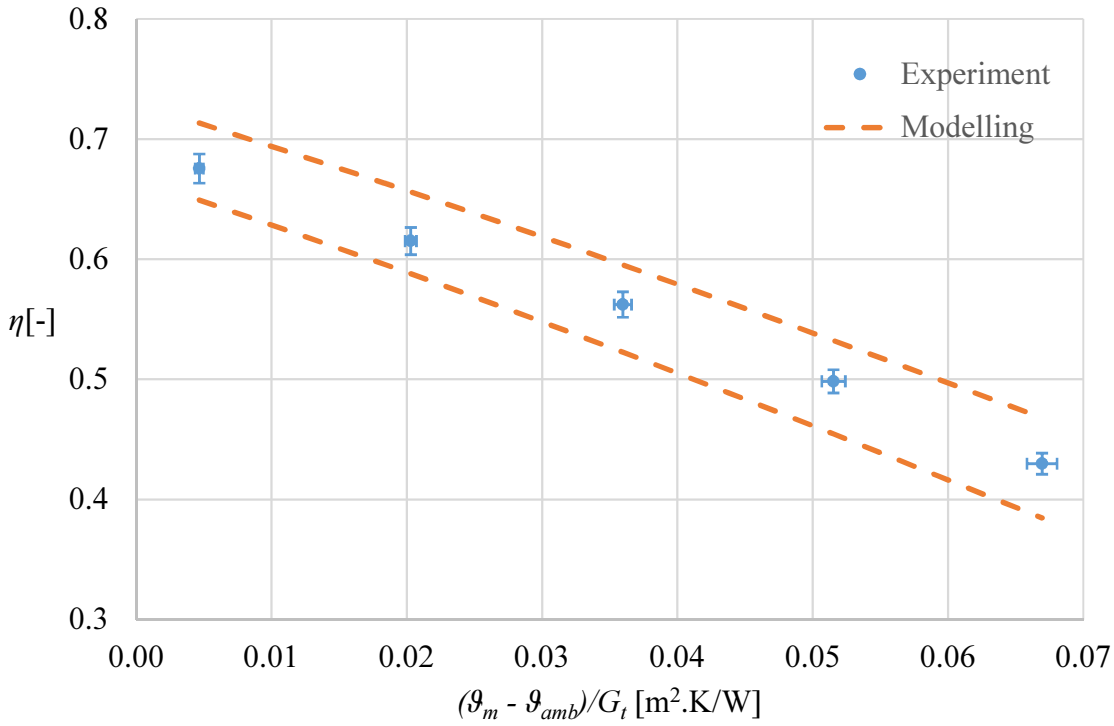

Fig. 15 – Experimental evaluation of the detailed theoretical model by collector testing (flat-plate collector № 4)

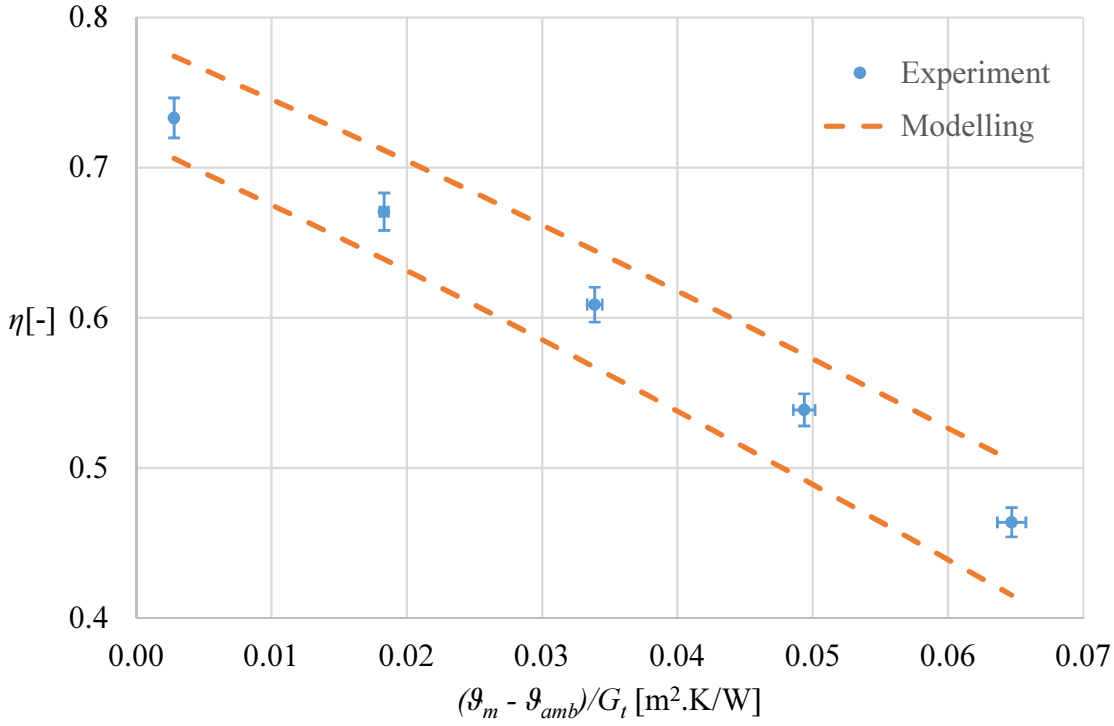

Fig. 16 – Experimental evaluation of the detailed theoretical model by collector testing (collector slope - 0°)

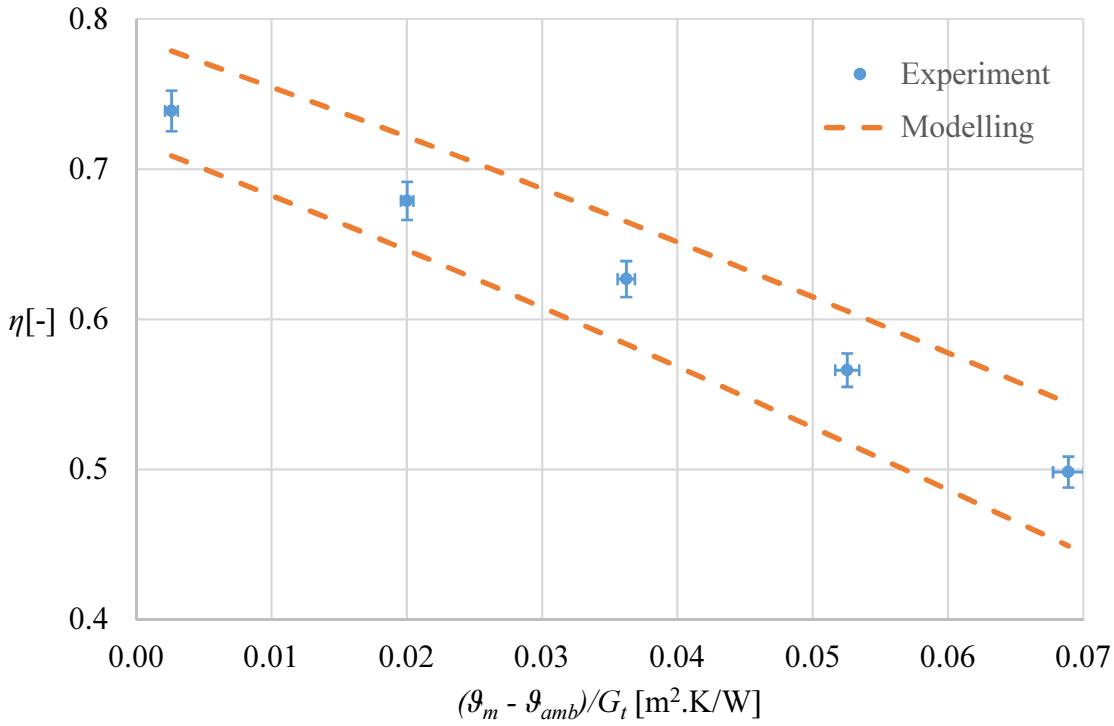

Fig. 17 – Experimental evaluation of the detailed theoretical model by collector testing (collector slope - 90°)

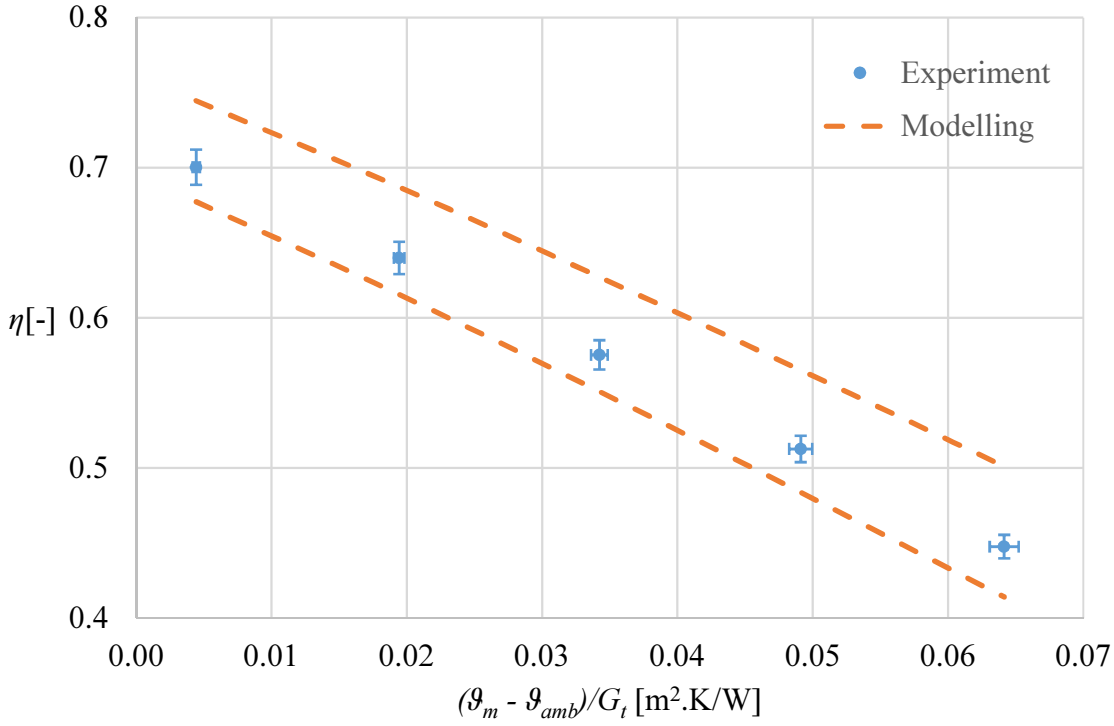

Fig. 18 – Experimental evaluation of the detailed theoretical model by collector testing (low flow)

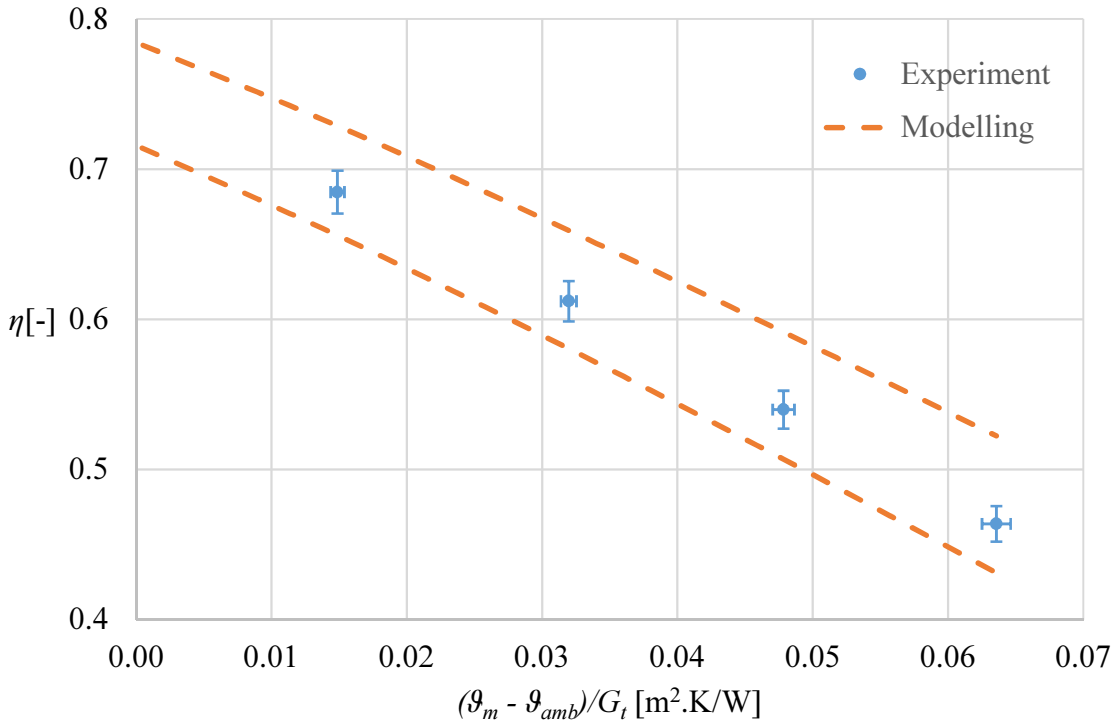

Fig. 19 – Experimental evaluation of the detailed theoretical model by collector testing (high flow)

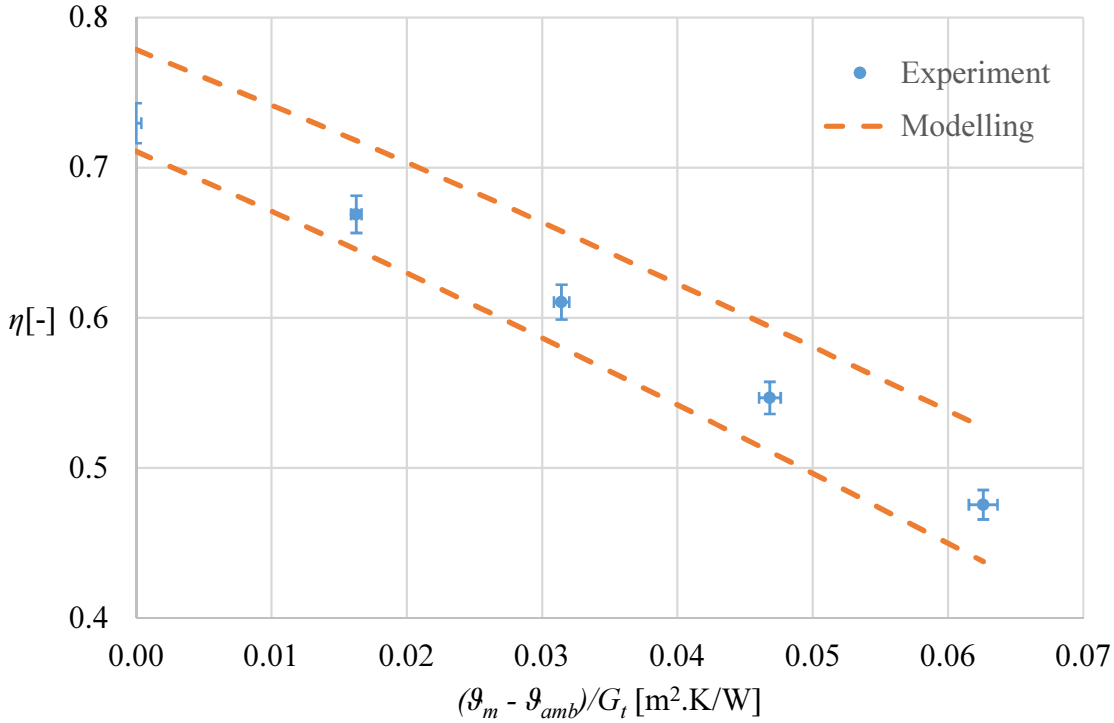

Fig. 20 – Experimental evaluation of the detailed theoretical model by collector testing (low wind)

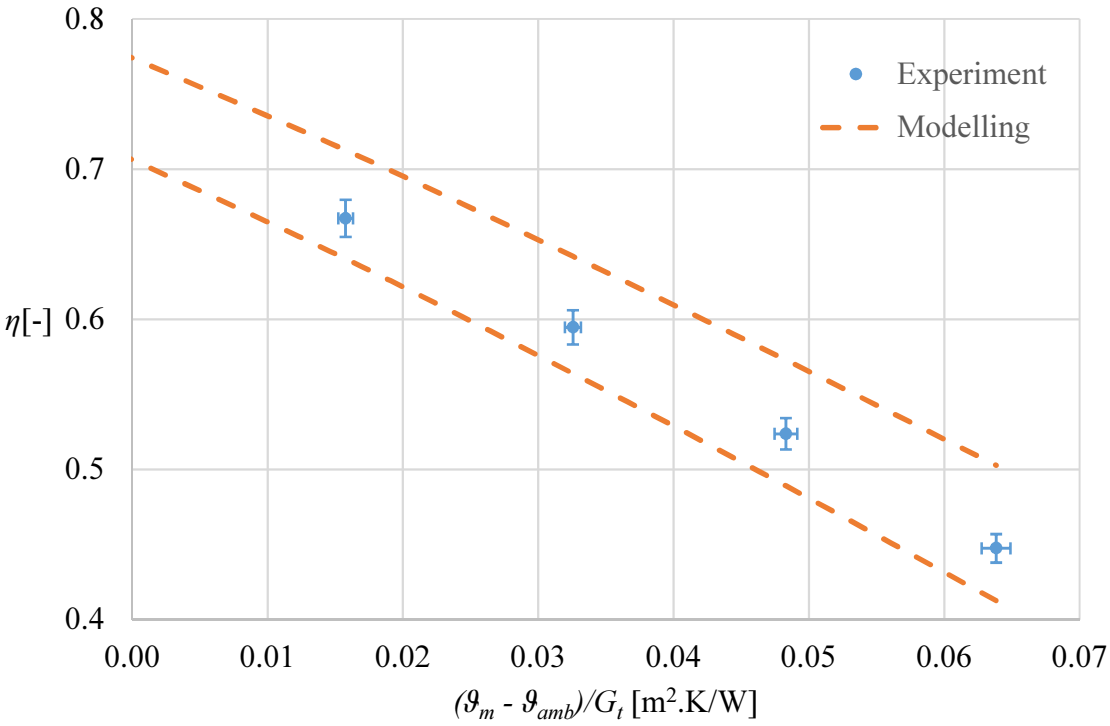

Fig. 21 – Experimental evaluation of the detailed theoretical model by collector testing (high wind)

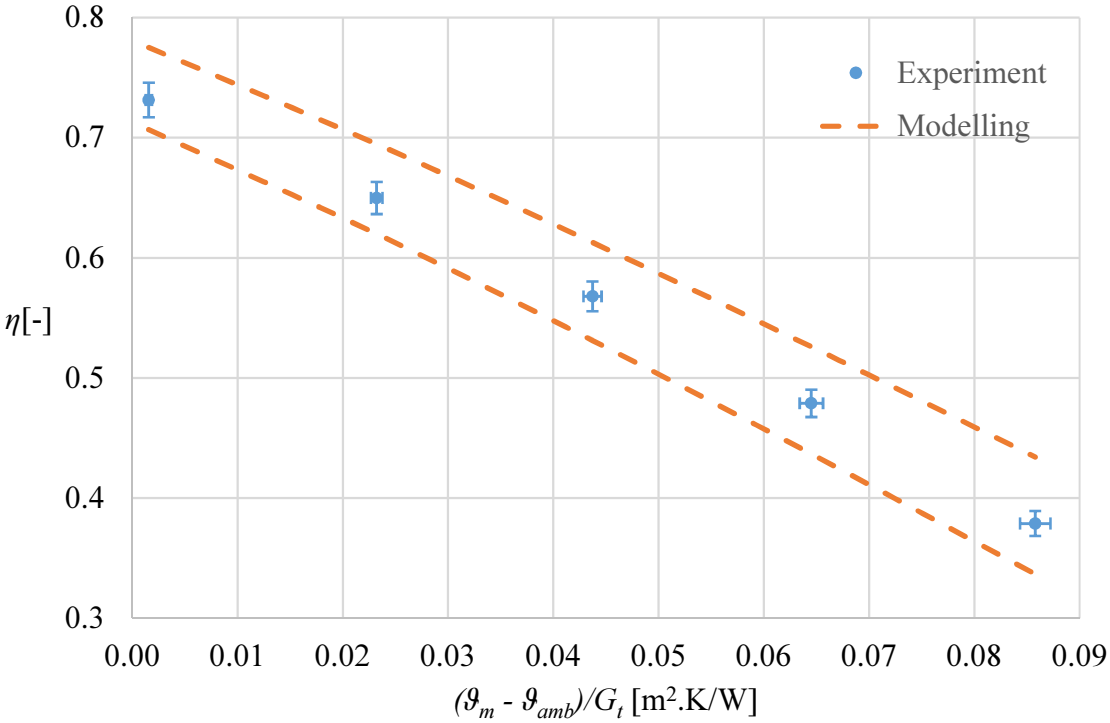

Fig. 22 – Experimental evaluation of the detailed theoretical model by collector testing (low radiation)

All figures show a good agreement between the modelled and experimentally obtained solar collector efficiency within the range caused by uncertainty of model input parameters (uncertain values of thermal properties of used materials, optical properties of surfaces, etc.). Because the large range of uncertainty of physical properties for collector components which results in large range of simulated performance the validation of model shall continue with solar collectors with more reliable inputs for individual components. This will be presented in future versions of this documents.

9 References

[1] Matuška T., Zmrhal V. A mathematical model and design tool KOLEKTOR 2.2 reference handbook. 2009.

[2] Hottel H., Woertz B. The performance of flate plate solar collector. Transactions of ASME, No. 64, pp. 91-104, 1942.

[3] Hottel H., Whillier A. Evaluation of flate-plate solar collector performance. Transactions of conference on the use of solar energy, pp 74-104, 1955.

[4] Bliss J. The derivations of several "plate-efficiency factors" usefull in the design of flate-plate heat collectors. Solar Energy, No. 3(4), pp. 55-64, 1959.

[5] Duffie J. A., Beckman W. A. Solar engineering of thermal processes. Wiley, 1991, 919 p.

[6] Matuška T. Transparent thermal insulations and there use in solar energy applications, Ph.D. thesis, CTU in Prague, 2013.

[7] McAdams, W.H. Heat Transmission, 3rd edition. McGraw-Hill, New York. pp.249. 1954.

[8] Jürges, W. Der Wärmeübergang an einer ebenen Wand, Behifte zum Gesundheits-Ingenieur, Reihe 1, Beiheft 19, München, 1924.

[9] Watmuff J.H., Charters, W.W.S, Proctor, D. Solar and wind induced external coefficients for solar collectors. Int. Revue d'Hellio-technique Vol. 2, pp. 56, 1977.

[10] Test, F. L., Lessmann, R. C.: An experimental study of heat transfer during forced convection over a rectangular body. Transactions of ASME – Journal of Heat Transfer, Vol. 102, 146-151, 1980.

[11] Test, F. L, Lessmann, R. C., Johary, A. Heat transfer during wind flow over rectangular bodies in the natural environment. ASME J. Heat Transfer 103, 262-267, 1981.

[12] Kumar, S., Sharma, V. B., Kandpal, T. C., Mullick, S. C. Wind induced heat losses from outer cover of solar collector. Renewable Energy, Vol. 10, No. 4, pp. 613-616, 1997.

[13] Hollands et al. Free convective heat transfer across inclined air layers. Transactions of ASME, Journal of Heat Transfer Vol. 98, pp. 189-193, 1976.

[14] Buchberg, H., Catton, I., Edwards, D. K. Natural convection in enclosed spaces - a review of application to solar energy collection. Transactions of ASME, Journal of Heat Transfer Vol. 98, pp. 182-188, 1976.

[15] Randall, K. R., Mitchell, J. W., El-Wakil, M. M. Natural convection heat transfer characteristics of flat-plate enclosures. Transactions of ASME, Journal of Heat Transfer Vol. 101, pp. 120-125, 1979.

[16] Schinkel W. M. M. Natural convection in inclined air-filled enclosures, ISBN 90-6231-079-6. ed. Dutch Efficiency Bureau 1980.

[17] Sazima, M., Kmoníček, V., Schneller, J. a kol. Technický průvodce - Teplo. SNTL Praha 1989. ISBN 80-03-00043-2.

[18] Arnold, J. N., Catton, I., Edwards, D. K. Experimental investigation of natural convection in inclined rectangular regions of differing aspect ratios. ASME Paper 75-HT-62, 1975.

[19] Shah, R. K., London, A. L. Laminar flow forced convection in ducts. 1st edition. New York. Academic Press. 1978.

[20] Hausen, C. H. Z. Ver. Dtsch. Ing. Beih. Verfahrenstech. Vol. 91, No. 4, 1934.

[21] Sieder, E. N., Tate, G. E. Heat transfer and pressure drop of liquids in tubes. Ind. Eng. Chem., Vol. 28, pp. 1429-1436, 1936.

[22] Churchill S. W. and Ozoe H. Correlations for laminar forced convection in flow over an isothermal flat plate and in developing and fully developed flow in an isothermal tube. Journal of Heat Transfer Vol. 95, pp. 416-419, 1973.

[23] Colburn, A. P. A method of correlating forced convection heat transfer data and a comparison with fluid friction. Transactions of AIChE, 29, 174, 1933.

[24] Dittus, P. W., Boelter, L. M. K. Heat transfer in automobile radiators of the tubular type. University of California Publications on Engineering, Vol. 2, No. 13, p. 443-461, Berkeley, 1930; reprinted in Int. Commun. Heat Mass Transfer, vol. 12, pp. 3-22, 1985.

[25] Kakac, S., Shah, R. K., Aung, W. Handbook of single-phase convective heat transfer, Wiley, New York, 1987.

[26] Petukhov, B. S., in T. F. Irvine and J. P. Hartnett, Eds. Advances in Heat transfer, Vol. 6, Academic Press, New York, 1970.

[27] Gnielinski, V. New equations for heat and mass transfer in turbulent pipe and channel flow, Int. Chem. Engineering. Vol. 16, pp. 359-368, 1976.

[28] Sleicher, C. A., Rouse, M. W. Convective Correlation for Heat Transfer to Constant and Variable Property Fluids in Turbulent Pipe Flow. Journal of Heat Transfer Vol. 18, pp. 677-683, 1975.

[29] Brandemuehl, M.J., Beckman, W.A. Transmission of diffuse radiation through CPC and flat-plate collector glazing. Solar Energy Vol. 24, pp. 511–513, 1980.

[30] ISO 9806:2013. Solar energy - Solar thermal collectors - Test methods. 2013.

[31] Mathioulakis, E., Vorostopoulos, K., Belessiotis, V. Assessment of Uncertainty in Solar Collector Modeling and Testing. Solar Energy 66, 337-347, 1999.

[32] Müller-Schöll, Ch., Frei, U. Uncertainty Analyses in Solar Collector Measurement. Proc. of Eurosun 2000, Copenhagen, 2000.

Appendix 1: Installation

The Type205 collector model is a TRNSYS 17 drop-in dll component. For a complete set of files one should have:

Type205.dll – the drop-in dll file

Type205.cpp – the C++ source code

Type205.tmf – the Simulation Studio proforma

Type205.bmp – the Simulation Studio proforma icon

For installation:

1. Copy the .dll file to \TRNSYS17\UserLib\ReleaseDLLs\

2. Copy the .tmf and .bmp files to the \Proformas folder, e.g. C:\Trnsys17\Studio\Proformas\Nonstandard\

3. Restart simulation studio if it was running.